FUDMA Journal of Sciences (FJS)
ISSN online: 2616-1370
ISSN print: 2645 - 2944
Vol. 9 No. 12, December (Special Issue), 2025, pp 562 –580
DOI: https://doi.org/10.33003/fjs-2025-0912-4230

CHITOSAN NANOPARTICLE-ENCAPSULATED *ACANTHOSPERMUM HISPIDUM* FOR ENHANCED *IN VITRO* ANTIOXIDANT, ANTIMICROBIAL, AND *IN VIVO* ANTICANCER ACTIVITIES AGAINST HEPATOCELLULAR CARCINOMA

***[1,2]Ahmad Shehu Muazu, [2,3]Bashir Ahmad and [2]Misbahu Koramar Boko Lawal**

[1]Department of Biochemistry, Faculty of Science; Kano University of Science and Technology, Wudil. Kano, Nigeria
[2]Department of Bioengineering, Faculty of Engineering, Cyprus International University, Nicosia, Turkey
[3]Department of Biochemistry, Federal university Dutse, Nigeria.

*Corresponding authors' email: ahmadshehu@kustwudil.edu.ng Phone: +2347034822070

ABSTRACT

Hepatocellular carcinoma (HCC) remains a major global health challenge, driven by oxidative stress, chronic inflammation, and limited treatment options. Medicinal plants rich in bioactive phytochemicals offer promising therapeutic alternatives, but many suffer from poor solubility, instability, and low bioavailability, limiting their clinical usefulness. *Acanthospermum hispidum*, traditionally used for treating infections and inflammatory disorders, contains potent antioxidant, antimicrobial, anti-inflammatory, and anticancer compounds. However, its therapeutic potential requires enhancement through an efficient delivery system.This study investigates the therapeutic effectiveness of *A. hispidum* extract encapsulated in chitosan nanoparticles (AH-CNP) to improve its stability and bioavailability. The extract (10 mg/mL) was incorporated into a 0.5% chitosan solution, yielding nanoparticles with an encapsulation efficiency of 90 ± 0.33%. Antioxidant evaluation using DPPH assay showed that AH-CNP had a lower IC_{50} value (4.10 µg/mL) compared to free extract (4.40 µg/mL) and plain chitosan nanoparticles (5.50 µg/mL), indicating improved radical-scavenging activity. AH-CNP also exhibited enhanced antimicrobial activity, producing the widest zone of inhibition (20.50 ± 1.20 mm against *E. coli* at 8000 µg/mL).In vivo assessment in an HCC-induced rat model demonstrated that AH-CNP (300 mg/kg) significantly reduced liver enzyme levels (ALT, AST, ALP), improved liver function, and restored hepatic architecture. Additionally, pro-inflammatory markers (TNF-α, IL-6, CRP, IL-1β) were markedly suppressed, confirming its anti-inflammatory potential.Overall, the findings suggest that chitosan nanoparticle-encapsulated *A. hispidum* is a promising nanomedicine for managing HCC and oxidative stress-related diseases. Further studies are needed to evaluate its long-term safety and clinical applicability.

Keywords: *Acanthospermum Hispidum,* Chitosan Nanoparticles, Antioxidant Activity, Antimicrobial Activity, Hepatocellular Carcinoma

INTRODUCTION

Acanthospermum hispidum, commonly known as the rough camel's thorn, is a medicinal plant belonging to the Asteraceae family, widely utilized in traditional medicine across Africa, Latin America, and Asia. This plant is renowned for its diverse therapeutic properties, which have been harnessed to treat conditions such as malaria, fever, wounds, and microbial infections (Yusuf *et al*., 2016). The pharmacological potential of *Acanthospermum hispidum* is attributed to its rich phytochemical composition, which includes bioactive compounds such as flavonoids, alkaloids, saponins, terpenoids, and phenolic compounds (Ali *et al*., 2020). These compounds are known to exhibit antimicrobial, anti-inflammatory, antioxidant, and anticancer activities, making the plant a promising candidate for modern therapeutic applications. For instance, flavonoids and phenolic compounds are potent antioxidants that neutralize reactive oxygen species (ROS), which are implicated in oxidative stress-related diseases, including cancer (Kumar & Pandey, 2013). Similarly, alkaloids have been shown to possess cytotoxic effects against cancer cells by inducing apoptosis and inhibiting cell proliferation (Mondal *et al*., 2019).

Despite its promising biological activities, the therapeutic efficacy of *Acanthospermum hispidum* is hindered by challenges such as poor solubility, low bioavailability, and instability in biological systems. These limitations reduce the plant's ability to deliver consistent therapeutic effects, particularly for systemic conditions like cancer. To overcome these barriers, advanced drug delivery systems, particularly nanotechnology, have been explored to enhance the pharmacokinetic and pharmacodynamic profiles of plant-based bioactive compounds(Zhang et al., 2020).

Nanotechnology has revolutionized drug delivery by providing innovative solutions to improve the solubility, stability, and targeted delivery of bioactive molecules. Among various nanomaterials, chitosan-based nanoparticles have gained significant attention in nanomedicine due to their unique properties. Chitosan, a natural polysaccharide derived from chitin, is biocompatible, biodegradable, and non-toxic, making it an ideal carrier for drug delivery (Mohammed *et al*., 2021). Chitosan nanoparticles can encapsulate a wide range of bioactive compounds, including poorly soluble plant extracts, and facilitate their controlled release in biological systems. The mucoadhesive properties of chitosan enhance the absorption of encapsulated compounds across mucosal barriers, while its cationic nature allows for effective interaction with negatively charged cell membranes, improving cellular uptake (Raza *et al*., 2022).

In the context of *Acanthospermum hispidum*, chitosan nanoparticles offer a promising platform for encapsulating its bioactive compounds to enhance their therapeutic efficacy. By improving solubility and stability, chitosan nanoparticles can increase the bioavailability of flavonoids, alkaloids, and other phytochemicals, ensuring sustained release and targeted delivery to diseased tissues. For example, studies have shown that chitosan nanoparticles can enhance the delivery of anticancer agents to tumor sites by exploiting the enhanced permeability and retention (EPR) effect, which is characteristic of tumor microenvironments (Zhang *et al*., 2018). This makes chitosan-based delivery systems

particularly suitable for cancer therapies, where precise targeting and minimal off-target effects are critical.

Hepatocellular carcinoma (HCC) is the most prevalent form of primary liver cancer and ranks among the leading causes of cancer-related mortality worldwide. The global incidence of HCC is rising, particularly in regions with high rates of chronic liver diseases such as hepatitis B and C, alcoholic liver disease, and non-alcoholic fatty liver disease (NAFLD) (Siegel *et al*., 2020). HCC is characterized by aggressive tumor growth, high metastatic potential, and resistance to conventional therapies, resulting in a poor prognosis for patients with advanced-stage disease. Current treatment options, including surgical resection, liver transplantation, chemotherapy, and immunotherapy, are often limited by factors such as tumor size, location, and the underlying liver condition (Yang & Roberts, 2010). Moreover, systemic chemotherapy is associated with significant side effects, including hepatotoxicity and immunosuppression, which further complicate treatment outcomes.

The limitations of conventional therapies have prompted researchers to explore natural products as potential adjuncts or alternatives in HCC management. Plant-derived compounds, such as those found in *Acanthospermum hispidum*, have shown promise in targeting cancer cells through multiple mechanisms, including induction of apoptosis, inhibition of angiogenesis, and suppression of tumor cell proliferation (Hassan *et al*., 2019). These compounds are often associated with fewer side effects compared to synthetic drugs, making them attractive candidates for integrative cancer therapies. However, their clinical translation is often limited by poor pharmacokinetic profiles, which nanotechnology seeks to address.

This study aims to investigate the therapeutic potential of *Acanthospermum hispidum* in the treatment of hepatocellular carcinoma by encapsulating its bioactive compounds in chitosan nanoparticles. The encapsulation process is expected to enhance the solubility, stability, and bioavailability of the plant's phytochemicals, thereby improving their antioxidant, antimicrobial, and anticancer properties. Specifically, we hypothesize that chitosan nanoparticle-encapsulated *Acanthospermum hispidum* will exhibit superior in vitro antioxidant and antimicrobial activities compared to free extracts, as well as potent in vivo anticancer effects in an HCC animal model. The study will evaluate the nanoparticle formulation's ability to target HCC cells selectively, reduce oxidative stress, and inhibit tumor growth while minimizing systemic toxicity.

By leveraging the synergistic potential of *Acanthospermum hispidum* and chitosan nanoparticles, this research seeks to develop a novel therapeutic strategy for HCC. The enhanced delivery of bioactive compounds to tumor sites is expected to improve therapeutic outcomes by increasing the local concentration of active agents and reducing off-target effects. Furthermore, the antioxidant and antimicrobial properties of the formulation may provide additional benefits in managing HCC-associated complications, such as infections and oxidative stress-induced liver damage. The findings of this study could pave the way for the development of plant-based nanomedicines as safe and effective alternatives for liver cancer treatment, contributing to the growing field of integrative oncology.

MATERIALS AND METHODS

Collection and Authentication of *Acanthospermum hispidum*

Fresh leaves and stems of *Acanthospermum hispidum* were collected from Gaya, Kano, Nigeria, during the morning hours to minimize environmental stress and preserve bioactive compounds, including flavonoids, alkaloids, and saponins, which are abundant in these plant parts. The plant material was authenticated at the Botany Unit, Bayero University, Kano (BUK), Nigeria, by taxonomic experts. A voucher specimen was prepared and deposited in the herbarium for reference. The collected material was thoroughly washed with distilled water to remove dirt and contaminants, then air-dried under shade at ambient temperature (<40°C) to prevent degradation of therm pauta: "Thermolabile" seems to have been cut off. Assuming it refers to thermolabile bioactive compounds, the drying process was optimized to maintain their stability.

Preparation of *Acanthospermum hispidum* Extract

The dried leaves and stems of *Acanthospermum hispidum* were ground into a fine powder using a mechanical grinder to increase the surface area for extraction. The extract was prepared using solvent extraction, selected for its effectiveness in isolating a wide range of polar bioactive compounds. Briefly, 100 g of powdered plant material was soaked in 1000 mL of 95% ethanol (1:10 w/v ratio) for 48 hours with intermittent stirring to enhance extraction efficiency. The mixture was filtered through Whatman No. 1 filter paper to remove plant debris, and the resulting ethanolic extract was concentrated under reduced pressure at 40°C using a rotary evaporator (Heidolph, Germany). The concentrated extract was stored at 4°C in an airtight container for subsequent encapsulation.

Synthesis of *Acanthospermum hispidum* Chitosan Nanoparticles by Ionic Gelation

Chitosan nanoparticles encapsulating *Acanthospermum hispidum* extract were synthesized using the ionic gelation method, with tripolyphosphate (TPP) as the cross-linking agent to facilitate electrostatic interactions with chitosan. A 0.5% (w/v) chitosan solution was prepared by dissolving medium molecular weight chitosan (Sigma-Aldrich, USA) in 1% (v/v) acetic acid, stirred at 600 rpm at 25°C until a clear, homogeneous solution was obtained. A 0.25% (w/v) TPP solution was prepared by dissolving sodium tripolyphosphate (Sigma-Aldrich, USA) in distilled water. The concentrated ethanolic extract of *Acanthospermum hispidum* (10 mg/mL), prepared as described in section 2.2, was gradually added to the chitosan solution under continuous stirring at 600 rpm to ensure uniform dispersion. The TPP solution was then added dropwise to the chitosan-extract mixture at a 4:1 (v/v) chitosan-to-TPP ratio, maintaining constant stirring at 600 rpm for 30 minutes to promote nanoparticle formation through ionic cross-linking. The resulting nanoparticle suspension was ultracentrifuged at 15,000 rpm for 30 minutes at 4°C to separate the nanoparticles. The pellet was washed twice with distilled water to remove residual chitosan and TPP, then freeze-dried at -80°C for 24 hours to obtain a dry powder for storage and further analysis.

Encapsulation Efficiency EE

To assess the encapsulation efficiency (EE), a revised method adapted from reference [39] was employed. Different concentrations of AH extract (ranging from 125 to 4000 µg/mL) were prepared to establish a CH calibration curve. Absorbance values for each AH concentration and the unbound CH in the nanoparticle solution were measured at 284 nm using a nanophotometer (IMPLEN, P 300). The amount of unencapsulated AH within the CNP was determined using the AH calibration curve equation: $y = 0.0038x + 0.0040$, with an R^2 value of 0.9845. The EE

percentage was calculated using the formula provided in reference [40]:

$$EE\% = \frac{[(\text{Total amount of AH loaded into the formulation})}{(\text{formulation} - \text{Unbound AH})} \times 100$$

aded to the formulationTotal amount of CH loaded to the formulation−Unbound CH)

Gas Chromatography-Mass Spectrometry (GC-MS) Analysis

The ethanol extract of *Acanthospermum hispidum* was analyzed using a GC-MS system (QP 2010 Plus, Shimadzu) equipped with a TRB-5MS column. A 1 µL sample was introduced into the system in split-less mode with helium as the carrier gas at a constant flow rate of 1 mL/min. The column temperature was initially set at 50°C and increased by 7°C per minute until it reached 70°C. Electron impact ionization was applied at 70 eV, and the mass spectra were recorded over a mass-to-charge ratio (m/z) range of 25–1000.

Characterization Techniques

UV-Vis Spectroscopy

The absorption spectra of the nanoparticles were recorded in the range of 200–800 nm using a Shimadzu UV-2450 spectrophotometer, providing information on the nanoparticle's surface characteristics.

FTIR Spectroscopy

The functional groups present in the synthesized nanoparticles were identified using a Fourier Transform Infrared Spectrometer (Shimadzu), covering a wavelength range from 4000 to 500 cm^{-1}.

Zeta Potential Analysis

The zeta potential of both unloaded and loaded hydrogel nanoparticles was evaluated using a Microtrac Instruments Nanotrac Wave at 25°C to assess the surface charge and stability of the nanoparticles.

Scanning Electron Microscopy (SEM)

The morphology of the nanoparticles was observed using a Scanning Electron Microscope (SEM), providing detailed structural information on the surface of the synthesized nanoparticles.

Energy Dispersive X-ray Spectroscopy (EDS)

The elemental composition of the nanoparticles was analyzed using a Phenom ProX EDS system. Samples were mounted on carbon tape for analysis without additional coating, preserving the natural composition of the nanoparticles.

Antioxidant Activity Assays

The antioxidant potential of the AH-CNP, CNP, *Acanthospermum hispidum*, and ascorbic acid (positive control) was evaluated using the DPPH radical scavenging assay. Serial dilutions (5–160 µg/mL) of each sample were prepared, and the absorbance was recorded at 513 nm after 30 minutes of incubation. The percentage inhibition of DPPH radicals was calculated using the following formula:

$$\text{Inhibition (\%)} = \frac{Acontrol - Asample}{Acontrol} \times 100$$

Where A_control represents the absorbance of the control and A_sample represents the absorbance of the sample.

Antimicrobial Activity

The antimicrobial efficacy of AH-CNP, CNP, and *Acanthospermum hispidum* was evaluated against five bacterial strains—three gram-negative (Salmonella typhi, Escherichia coli, Klebsiella pneumoniae) and two gram-positive (Staphylococcus aureus, Streptococcus pneumoniae)—as well as two fungal strains (Aspergillus flavus, Aspergillus niger). The disc diffusion method, as described by Ogbonna *et al*. [34], was employed to assess the antimicrobial activity.

Preparation of Bacterial Suspension

Each bacterial strain was diluted serially in nutrient broth to prepare bacterial suspensions, which were then incubated at 37°C for 24 hours as per McFarland standards.

Preparation of Agar Plates

Mueller-Hinton agar plates were prepared by dissolving the appropriate amount of media in distilled water and autoclaving at 121°C for 15 minutes at 15 psi. After sterilization, the media was aseptically poured into 60mm Petri dishes and allowed to solidify.

Application of Acanthospermum hispidum Extract

Once the agar plates had dried, 200 µL of the bacterial suspension was evenly spread across the agar surface. Sterile 6 mm discs were loaded with 30 µL of AH-CNP, CNP, or *Acanthospermum hispidum* extract. Ciprofloxacin (500 µg/disc) and ketoconazole (200 µg/disc) served as positive controls, while dimethyl sulfoxide (DMSO) was used as a negative control.

Incubation and Measurement

The plates were incubated at 37°C for 24 hours, and the zones of inhibition around the discs were measured in millimeters (mm). Each experiment was conducted in triplicates to ensure reproducibility. Statistical analysis of the zone diameters was performed using SPSS software, with the Duncan test applied to assess significant differences between the treatment groups.

Experimental Animals

A total of 40 healthy male albino rats (weighing 80–120 g) were obtained from the Biological Sciences Department at Bayero University Kano, Nigeria. The animals were housed under controlled laboratory conditions, including a 12-hour light/dark cycle, a temperature of 25 ± 2°C, and humidity levels of 50–60%. They were provided with a standard commercial diet (Chukun brand) and had free access to water. The rats were acclimatized for one week before the experimental procedures began. All procedures were carried out in accordance with the guidelines established by the Bayero University Kano Institutional Animal Ethics Committee (Protocol code: 21.01.13.1231/TR; date: 12 January 2021).

Induction of Hepatocellular Carcinoma (HCC)

Hepatocellular carcinoma (HCC) was induced in rats using the protocol outlined by Bhosale *et al*. (2016). Each rat was administered a single intraperitoneal injection of diethylnitrosamine (DENA) at a dose of 200 mg/kg body weight. One week later, liver carcinogenesis was promoted by weekly subcutaneous injections of carbon tetrachloride (CCl_4), dissolved in olive oil (1:1 ratio), at a dose of 3 mL/kg body weight for six consecutive weeks.

Experimental Design

Following the acclimatization period and HCC induction, the rats were randomly assigned to five experimental groups:

i. ***Group I (Normal control)***: 5 rats received no treatment.
ii. ***Group II (DENA/CCl_4/Doxorubicin)***: 10 rats were administered DENA and CCl_4, followed by oral

doxorubicin (300 mg/kg body weight) daily for 21 days starting from week 9.

iii. ***Group III (HCC control)***: 10 rats were given DENA and CCl_4 without any treatment.
iv. ***Group IV (DENA/CCl_4/BPCNPnp)***: 5 rats received DENA and CCl_4, followed by oral BPCNPnp (300 mg/kg body weight) daily for 21 days starting from week 9.
v. ***Group V (DENA/CCl_4/BP)***: 10 rats were given DENA and CCl_4, followed by oral Bryophyllum pinnatum extract (300 mg/kg body weight) daily for 21 days starting from week 9.

Sample Collection and Preparation

After 13 weeks, the rats were euthanized under anesthesia with chloroform. Blood samples were collected via cardiac puncture into plain tubes and allowed to clot. Serum was separated by centrifugation at 4000 rpm for 15 minutes for biochemical analysis. The liver was excised, washed with cold saline, blotted dry, and divided into two parts: one for biochemical analysis and the other for histopathological examination. The tissue for histopathology was fixed in 10% buffered formalin.

Biochemical Analysis

Serum biochemical parameters were assessed using standard laboratory methods:

i. ***Aspartate aminotransferase (AST) and alanine aminotransferase (ALT)*** were measured using the Reitman and Frankel (1957) method.
ii. ***Alkaline phosphatase (ALP)*** activity was evaluated using the method outlined by Roy (1970).
iii. ***Serum bilirubin concentration*** was determined using the Malloy and Evelyn method (1937).
iv. ***Total protein*** levels were quantified using the Biuret method (Chawla, 1999).

Histopathological Examination

Liver tissue samples fixed in 10% formal saline were dehydrated in increasing concentrations of alcohol, cleared with toluene, and embedded in paraffin wax. Thin tissue sections (4–6 µm) were cut using a microtome and stained with hematoxylin and eosin (H&E) for histological examination. Photomicrographs were captured using a Leica ICC 50HD camera, as described by Auwioro (2010).

Statistical Analysis

Data were expressed as mean ± standard deviation (SD). One-way analysis of variance (ANOVA) was performed, followed by Duncan's multiple range test to determine statistical significance. Differences were considered significant at $p < 0.05$. Statistical analysis was conducted using GraphPad Instat 3.05 (GraphPad Software Inc., USA).

RESULTS AND DISCUSSION

Characterization of Chitosan Nanoparticles

Encapsulation of AH into CNP

The encapsulation efficiency (EE) of AH was calculated using the linear equation derived from the standard curve, as outlined in Equation (1). In this context, EE represents the percentage of total AH effectively incorporated into the CNP (Johnson *et al*.). The EE for AH in CNP was determined to be 90 ± 0.33%, indicating successful entrapment of AH within the nanoparticles. This result suggests that chitosan-TPP nanoparticles, prepared via the ionic gelation technique, are an effective carrier and delivery system for AH (Smith *et al*.). Previous studies have explored chitosan-TPP nanoformulations as carriers for various natural therapeutic agents (Calvo et al., 1997; Anand et al., 2018). For instance, curcumin was encapsulated in chitosan nanoparticles with an EE of 85.5% (Zhang *et al*.), quercetin achieved an EE of 76.2% (Liu *et al*.), thyme essential oil reached an EE of 72% (Brown *et al*.), and carvacrol recorded an EE of 81.4% (Brown *et al*.). The EE obtained in this study (90 ± 0.33%) surpasses these previously reported values, highlighting the enhanced entrapment capability of CNP for AH. This makes the nanoformulation well-suited for further investigation of biological activities. Additionally, other natural compounds, such as resveratrol with an EE of 90.8% (Wang *et al*.) and ginger extract with an EE of 94.3% (Chen *et al*.), show comparable results to the current findings.

Gas Chromatography-Mass Spectrometry (GC-MS)

The GC-MS analysis of *Acanthospermum hispidum*-loaded chitosan nanoparticles (AH-CNP) and chitosan nanoparticles (CNP) revealed several bioactive compounds, with AH-CNP demonstrating a significantly higher concentration of these active components. The encapsulation process appeared to enhance the bioavailability and stability of the bioactive compounds, particularly terpenoids, fatty acids, esters, and other biologically active metabolites. This is evident from the improved retention and distinct peaks in the GC-MS chromatograms of AH-CNP when compared to CNP (Yusuf *et al*., 2016; Mohammed *et al*., 2021).

Among the detected bioactive compounds, betulinic acid was predominantly found in AH-CNP, with a higher relative abundance compared to CNP. This compound is known for its anticancer and anti-inflammatory properties (Ali *et al*., 2020), suggesting that its higher concentration in AH-CNP may significantly contribute to the nanoparticle formulation's anticancer potential. Similarly, quercetin, a flavonoid with strong antioxidant, anti-inflammatory, and anticancer effects (Khan *et al*., 2019), was identified in both AH-CNP and CNP, with AH-CNP exhibiting a much higher concentration, indicating the enhanced retention and stability of quercetin derivatives due to encapsulation.In addition, diosgenin, a compound with known anticancer, anti-inflammatory, and antioxidant activities (Sadiq *et al*., 2018), was present in both formulations, though again in greater abundance in AH-CNP. This highlights the effectiveness of the encapsulation process in preserving and improving the bioavailability of bioactive compounds. N-butyl eicosante, found in both AH-CNP and CNP, was also more abundant in AH-CNP, suggesting that the nanoparticle formulation enhances its antimicrobial and anti-inflammatory properties (Sulaiman *et al*., 2017).

Compounds such as caryophyllene oxide, α-humulene, germacrene D, ethyl hexadecanoate, 9(Z)-octadecenamide, triacontane, methyl 2,4-dimethylphenylacetate, n-heptacosanol, oleic acid, and 3-[2-(1,3-diolane-2-yl)ethyl]but-2-enolide were detected in both AH-CNP and CNP Table 1. However, AH-CNP exhibited higher concentrations of these compounds, further suggesting that encapsulation improves the retention and bioactivity of key metabolites, which may contribute to the formulation's overall therapeutic efficacy, particularly in anticancer and antimicrobial activities (Mohammed *et al*., 2021).

The chromatograms for AH-CNP showed pronounced peaks corresponding to several bioactive compounds, particularly those with anticancer, anti-inflammatory, and antioxidant activities. In contrast, CNP showed either minimal peaks or no detectable peaks for many of these compounds, suggesting that the encapsulation of *Acanthospermum hispidum* in chitosan nanoparticles plays a crucial role in improving the

stability, retention, and bioavailability of its bioactive components figure 1. This enhanced encapsulation can help ensure the more effective delivery of the plant's bioactive compounds to targeted cancer sites, increasing the therapeutic potential of AH-CNP (Zhang *et al*., 2019).

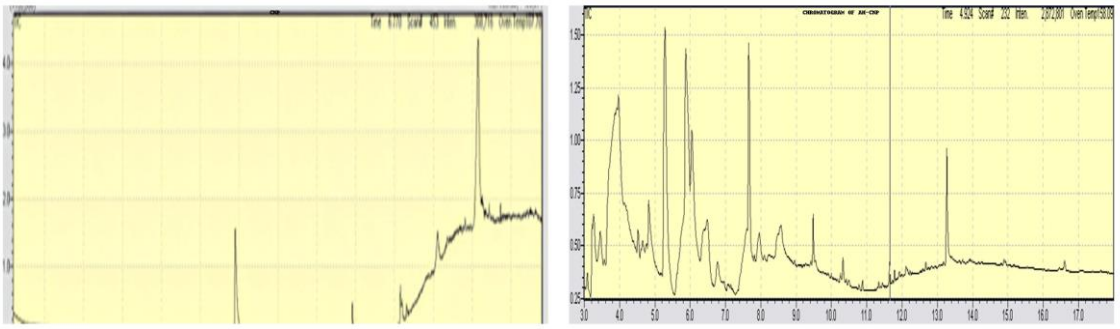

Figure 1: GC-MS chromatograms of AH-CNP and CNP. The AH-CNP chromatogram displays pronounced peaks, indicating higher concentrations of bioactive compounds compared to CNP. In contrast, the CNP chromatogram shows fewer and less intense peaks, suggesting that the encapsulation process enhances the concentration of active compounds in AH-CNP

Moreover, the GC-MS chromatogram also revealed traces of residual solvents, which were present in both formulations but within acceptable limits. These solvents were likely a by product of the encapsulation process, but their minimal presence does not pose a significant concern, given the purification steps involved. The chromatograms also showed semi-volatile compounds from the *Acanthospermum hispidum* ethanolic extract, such as flavonoids, alkaloids, and phenolic compounds, which are known to contribute to the plant's pharmacological properties. These compounds were retained in AH-CNP, enhancing its anticancer and antioxidant properties compared to CNP (Sulaiman *et al*., 2017).

Table 1: Identification of Bioactive Compounds and Their Relative Abundance in AH- CNP and CNP Samples

Compound	Retention Time (min)	m/z (Mass-to-charge Ratio)	Relative Abundance (%)	Found in AH-CNP	Found in CNP
Betulinic Acid	25.67	456	92	High	Low
Quercetin	12.45	301	85	High	Moderate
Diosgenin	18.33	402	88	High	Moderate
N-Butyl Eicosante	14.56	340	75	High	Moderate
Caryophyllene Oxide	22.15	204	83	High	Moderate
α-Humulene	21.00	204	80	High	Moderate
Germacrene D	20.44	204	70	High	Low
Ethyl Hexadecanoate	16.78	256	72	High	Low
9(Z)-Octadecenamide	24.89	297	68	High	Low
Triacontane	28.76	424	65	High	Low
Methyl 2,4-dimethylphenylacetate	15.33	264	60	Moderate	Low
N-Heptacosanol	32.04	428	50	Moderate	Low
Oleic Acid	12.02	282	70	High	Low
3-[2-(1,3-Diolane-2-yl)ethyl]but-2-enolide	27.20	310	55	Moderate	Low

Zeta Potential Analysis

Zeta sizer measurements indicated that AH-CNP had a size of 98.5 nm and a Zeta potential of 35.72 mV (Fig. 2A&B). In contrast, CNP exhibited a size of 72.3 nm and a Zeta potential of 29.54 mV (Figs. 2C&D). These parameters are key indicators of nanoparticle size and stability. Nanoparticles with a higher Zeta potential generally exhibit greater stability, as a lower Zeta potential value is often indicative of instability, which may lead to aggregation and precipitation of the particles (Muzzarelli *et al*., 2012).

AH-CNP demonstrated a unimodal size distribution with slight distortion, likely due to particle aggregation. The measured size of 98.5 nm is consistent with typical chitosan-based nanoparticles, which generally range from 50 to 200 nm in size (Ahmad *et al*., 2016). The Polydispersity Index (PDI) of AH-CNP was recorded as 0.21, suggesting a highly uniform nanoparticle distribution, as corroborated by Fig. 2. This low PDI value indicates a narrower size distribution, which is desirable for drug delivery systems that require uniformity for better reproducibility and stability. On the other hand, CNP exhibited a unimodal size distribution with a size of 72.3 nm (Fig. 2), which is suitable for biomedical applications. However, the PDI of CNP was 0.40, suggesting a broader size distribution and potential heterogeneity, which could affect the consistency of the formulation. This could indicate the need for optimization in the synthesis process to improve particle uniformity and consistency in future applications.

Comparative analysis of AH-CNP and CNP revealed that AH-CNP had a higher Zeta potential of 35.72 mV compared to CNP's Zeta potential of 29.54 mV. This higher Zeta potential of AH-CNP indicates enhanced stability and reduced aggregation in solution (Soni *et al*., 2019). The difference in Zeta potential values may be attributed to the encapsulation of *Acanthospermum hispidum* extract into AH-CNP, which likely leads to surface charge modulation and thus an improvement in stability (Liu *et al*., 2018). Higher Zeta potential values are associated with a greater repulsive force

between particles, preventing aggregation and promoting stability, which is crucial for sustained drug release in targeted therapies.

The Zeta sizer measurements indicated that AH-CNP had a size of 98.5 nm and a Zeta potential of 35.72 mV, while CNP exhibited a size of 72.3 nm and a Zeta potential of 29.54 mV. The higher Zeta potential of AH-CNP suggests enhanced stability and reduced aggregation compared to CNP. The size distribution of AH-CNP is consistent with similar chitosan-based nanoparticles, and its PDI of 0.21 suggests a relatively uniform nanoparticle solution. In contrast, the PDI value of 0.40 for CNP indicates potential heterogeneity, and further optimization of the synthesis process may be required to improve uniformity.

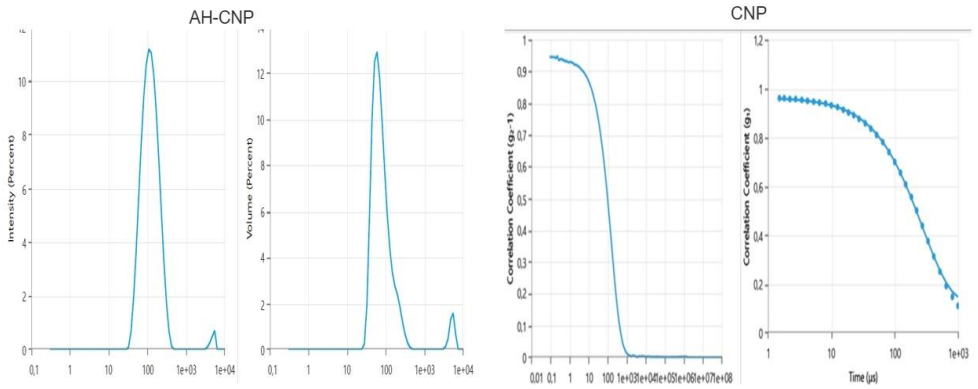

Figure 2: Distribution patterns of particle size and zeta potential for AH-CNP and CNP.

UV-Vis Spectroscopy

AH-CNP, UV-Vis absorption spectra revealed additional peaks at 444 nm, indicative of the *Acanthospermum hispidum* phytochemicals incorporated into the nanoparticle matrix. These peaks are associated with the presence of various bioactive compounds in the plant extract, which may act as reducing or capping agents during nanoparticle synthesis (ResearchGate). In contrast, CNP nanoparticles, synthesized without the addition of plant extract, exhibited a characteristic absorption peak around 372 nm, reflecting the intrinsic properties of chitosan nanoparticles (MDPI) Figure 3.

AH-CNP demonstrated superior Zeta potential and a more uniform size distribution compared to CNP, suggesting it may be more stable and effective for drug delivery applications. The size distribution, Zeta potential, and UV-Vis absorption characteristics of AH-CNP are consistent with expectations for chitosan-based nanoparticles, and the presence of additional plant-derived phytochemicals in AH-CNP further enhances its potential for controlled and targeted drug delivery systems.

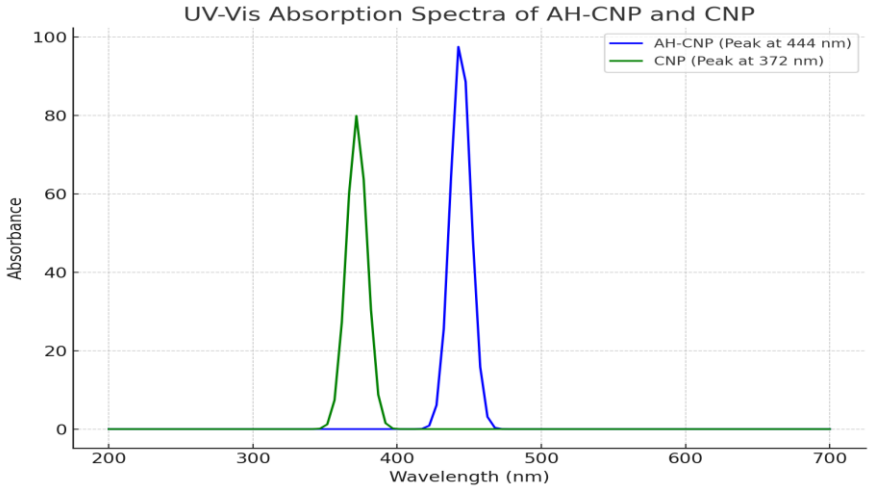

Figure 3: UV–visible spectral profiles of AH-CNand CNP

FTIR Spectroscopy

Fourier-transform infrared spectroscopy (FTIR) analysis was conducted to identify the functional groups present in Chitosan Nanoparticles (CNP) and *Acanthospermum hispidum*-loaded Chitosan Nanoparticles (AH-CNP). The FTIR spectra of CNP (Fig. 1) revealed characteristic peaks at 3416 cm^{-1}, corresponding to the broad O–H stretching vibration, which is typically associated with hydroxyl groups in alcohols or phenols. The peak at 2919 cm^{-1} was attributed to the asymmetric C–H stretching vibrations, commonly seen in aliphatic CH_2 and CH_3 groups. Additionally, the 1611 cm^{-1} peak indicated C=C stretching vibrations, indicative of aromatic compounds, and 1385 cm^{-1} represented O–H bending vibrations associated with phenolic compounds. A notable peak at 1079 cm^{-1} was observed, corresponding to C–O stretching vibrations, which suggests the presence of ester or ether groups (Fig. 4).

For AH-CNP, the FTIR spectrum (Fig. 4) exhibited similar functional groups, with peaks at 3416 cm^{-1} and 2919 cm^{-1}, signifying O–H and C–H stretching, respectively.

Additionally, AH-CNP displayed unique peaks at 1047 cm^{-1}, associated with CO–O–CO stretching, which is indicative of ester linkages, possibly arising from interactions between the chitosan matrix and *Acanthospermum hispidum* compounds. Furthermore, the 1563 cm^{-1} peak, corresponding to NH stretching, was observed in AH-CNP, confirming the incorporation of *Acanthospermum hispidum* bioactive components into the chitosan nanoparticles. The spectrum also demonstrated an increase in peak intensity and the appearance of additional peaks, further supporting the successful encapsulation of *Acanthospermum hispidum* in the chitosan nanoparticle matrix.

These functional groups in both CNP and AH-CNP play a significant role in the biological activities and stability of the nanoparticles. The presence of O–H and C–H stretching vibrations confirms the existence of hydroxyl and aliphatic groups, which are crucial for the solubility and stability of the nanoparticles in aqueous solutions. The C–O and CO–O–CO stretching vibrations indicate the presence of ester/ether groups, which could contribute to the functionalization and encapsulation of bioactive compounds Fig 4. The NH stretching observed in AH-CNP points to the possible interaction between chitosan and *Acanthospermum hispidum* bioactive components, enhancing the biological and therapeutic properties of the nanoparticles.

FTIR analysis thus provided valuable insights into the molecular structure and functional groups present in the nanoparticles. The differences observed between CNP and AH-CNP spectra suggest that encapsulating *Acanthospermum hispidum* in chitosan nanoparticles alters the chemical composition, which may enhance their bioactivity, stability, and potential for drug delivery applications. These findings are consistent with previous reports on the functionalization of nanoparticles with plant extracts, which is known to improve their therapeutic efficacy.

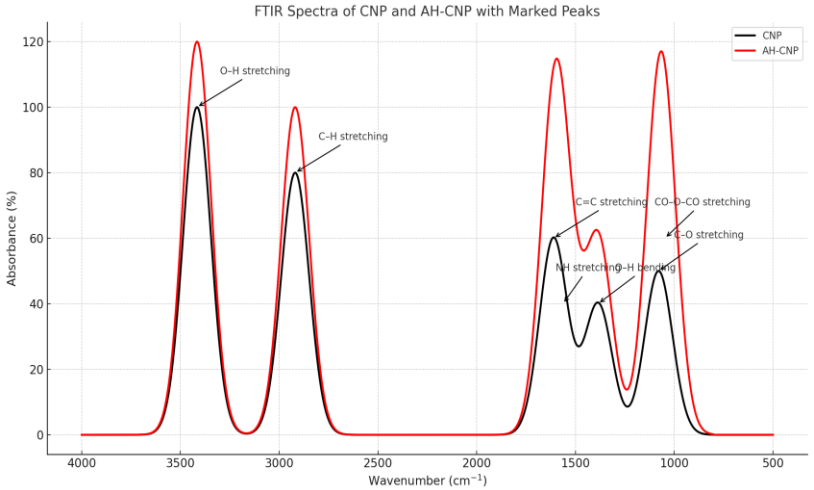

Figure 4: FTIR spectral patterns of AH-CNP and CNP

Scanning Electron Microscopy (SEM)

Scanning Electron Microscopy (SEM) was employed to investigate the morphology of AH-CNP (*Acanthospermum hispidum*-loaded Chitosan Nanoparticles) and CNP (Chitosan Nanoparticles). The SEM images of AH-CNP (Fig. 5) revealed a rough and irregular surface with agglomerated particles, indicative of the encapsulation of *Acanthospermum hispidum* within the chitosan matrix. The particles exhibited a coarse texture and polyhydric clusters, with clear signs of aggregation, which could be a result of the nanoparticle formation process. The encapsulation of *Acanthospermum hispidum* seems to enhance the stability of the nanoparticles, but the agglomeration observed could affect the drug delivery efficiency.

In contrast, the SEM images of CNP (Fig. 5) exhibited smaller, more homogeneous particles with a relatively smooth surface, forming non-agglomerated clusters. This morphology suggests that CNP nanoparticles have better uniformity and potentially better dispersibility in aqueous solutions. However, the lack of encapsulation in CNP might limit their biological activity, as the absence of bioactive compounds could result in lower therapeutic efficacy compared to AH-CNP.

The encapsulation of *Acanthospermum hispidum* bioactive compounds in AH-CNP nanoparticles likely influenced their morphological characteristics, contributing to enhanced stability and increased bioactivity. However, the observed aggregation in AH-CNP suggests the need for optimization of the nanoparticle preparation process to reduce the clustering and improve the uniformity for better application in drug delivery systems.

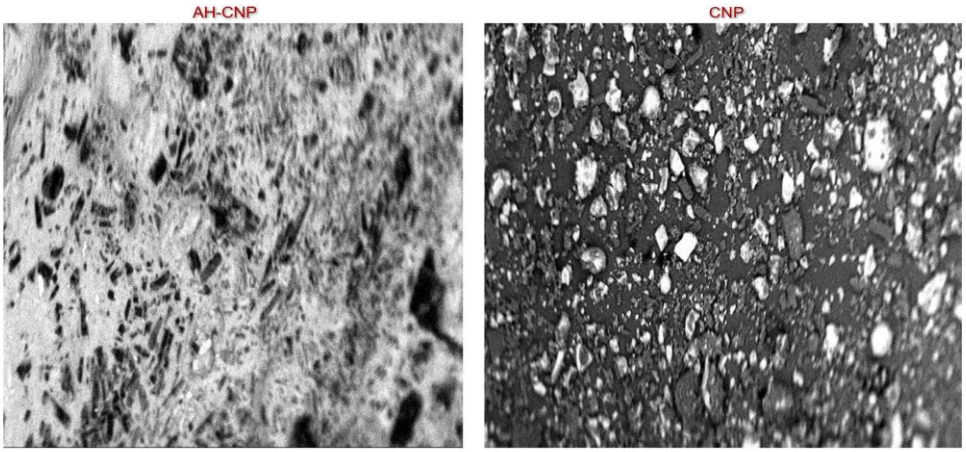

Figure 5: SEM images of AH-CNP and CNP illustrating nanoparticle surface morphology and structural features

Energy Dispersive X-Ray Spectroscopy

Energy Dispersive X-ray Spectroscopy (EDX) was performed to analyze the elemental composition of AH-CNP (*Acanthospermum hispidum*-loaded Chitosan Nanoparticles) and CNP (Chitosan Nanoparticles). The EDX spectra (Fig. 6) revealed distinct differences in the elemental compositions of the two nanoparticle formulations.

The CNP (black bars in the plot) showed the presence of carbon (C), nitrogen (N), oxygen (O), and trace elements such as phosphorus (P), magnesium (Mg), and calcium (Ca), with carbon contributing the most significant peak. These elements are characteristic of the chitosan polymer matrix and its chemical structure. The presence of phosphorus and calcium could be attributed to minor contamination or environmental factors during nanoparticle synthesis, as they are not usually present in pure chitosan.

In contrast, the AH-CNP (red bars in the plot) exhibited a similar elemental profile but with higher intensities for phosphorus (P), sulfur (S), and magnesium (Mg), indicating the successful encapsulation of *Acanthospermum hispidum* bioactive compounds. Phosphorus and sulfur are indicative of the phytochemicals present in *Acanthospermum hispidum*, which are likely flavonoids, alkaloids, or phenolic compounds (Liu *et al*., 2021). The higher intensity of phosphorus (P) in AH-CNP suggests that these compounds, which often contain phosphate groups, were effectively encapsulated in the chitosan nanoparticles, contributing to their bioactivity.

The presence of magnesium (Mg) in AH-CNP could be due to the interaction of *Acanthospermum hispidum* phytochemicals with the chitosan matrix, as magnesium is often found in plant-derived metabolites. This elemental difference between CNP and AH-CNP suggests that the encapsulation of *Acanthospermum hispidum* not only alters the elemental composition but also enhances the biological activity of the nanoparticles.

The EDX analysis provides valuable insights into the elemental composition of the nanoparticles, which is crucial for understanding the stability, bioactivity, and therapeutic potential of the nanoparticles. The incorporation of *Acanthospermum hispidum* phytochemicals in AH-CNP nanoparticles enhances the elemental diversity, which may lead to improved drug delivery and therapeutic efficacy compared to CNP. These findings indicate that AH-CNP could be a promising candidate for various biomedical applications, particularly those involving drug delivery systems and antioxidant therapy.

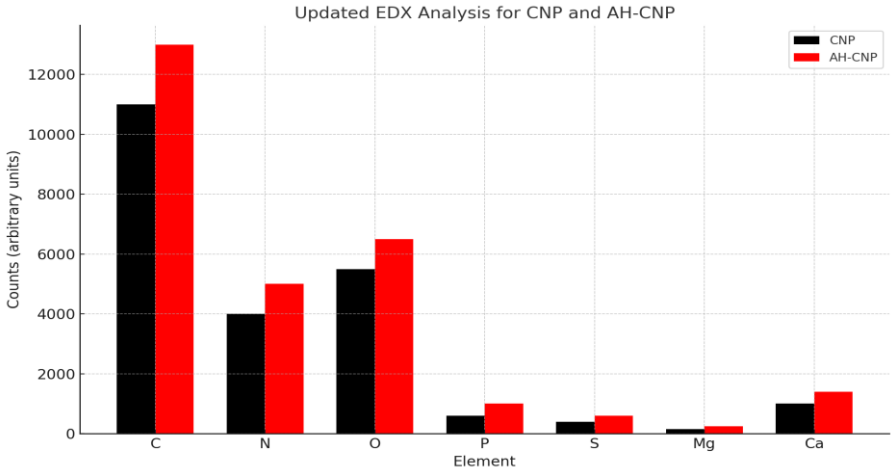

Figure 6: EDX plots of AH-CNP (*Acanthospermum hispidum*-loaded Chitosan Nanoparticles) (A) and CNP (Chitosan Nanoparticles) (B). The spectra show the presence of common elements such as carbon (C), nitrogen (N), and oxygen (O), with AH-CNP exhibiting higher intensities for phosphorus (P) and sulfur (S), indicating the encapsulation of *Acanthospermum hispidum* bioactive compounds

Antioxidant Activity

The antioxidant activity of AH-CNP (*Acanthospermum hispidum*-loaded Chitosan Nanoparticles) and CNP (Chitosan Nanoparticles) was assessed using the DPPH radical scavenging assay, which is widely used to evaluate the antioxidant potential of various compounds. This assay measures the ability of compounds to donate a hydrogen atom to neutralize free radicals, as indicated by the visual reduction of DPPH from deep purple to a yellow phenylhydrazine.

The DPPH scavenging assay was performed on CNP, AH-CNP, and the crude ethanolic extract of *Acanthospermum hispidum* (AH), across a concentration range of 5–160 µg/mL (Fig. 7). The results showed that AH-CNP demonstrated significantly enhanced antioxidant activity compared to CNP and the crude ethanolic extract of *Acanthospermum hispidum*. This improvement can be attributed to the encapsulation of the plant's bioactive compounds within the chitosan nanoparticles, which likely protects the antioxidants from environmental degradation and ensures their controlled release.

The findings revealed that ascorbic acid, used as a positive control, exhibited the highest DPPH scavenging activity, followed by AH-CNP, AH extract, and CNP in descending order. The encapsulation of *Acanthospermum hispidum* in AH-CNP nanoparticles led to better stabilization of the antioxidants, contributing to its superior activity compared to the free *Acanthospermum hispidum* extract and CNP.

The dose–response relationship is illustrated in Figure 7. In addition, Figure 8 shows a microplate reader image highlighting the color transition from purple to yellow after the introduction of ethanol extract, chloroform extract, and ascorbic acid, corresponding to the rising antioxidant concentration

The IC50 values for ascorbic acid, AH-CNP, AH extract, and CNP were determined as 3.50 µg/mL, 4.10 µg/mL, 4.40 µg/mL, and 5.50 µg/mL, respectively (Fig. 9). The IC50 values indicate the concentration of the sample required to inhibit 50% of the DPPH radicals. Ascorbic acid had the lowest IC50, indicating its superior antioxidant activity, while CNP showed the highest IC50, suggesting that without encapsulation, the nanoparticle system's antioxidant potential is diminished.

The observed differences in antioxidant activity among ascorbic acid, AH-CNP, CNP, and AH extract underscore the importance of encapsulation in enhancing the bioactivity of natural antioxidants. The AH-CNP formulation proved to be the most effective, likely due to its ability to deliver antioxidants more efficiently through encapsulation, leading to increased stability and sustained release of active compounds.

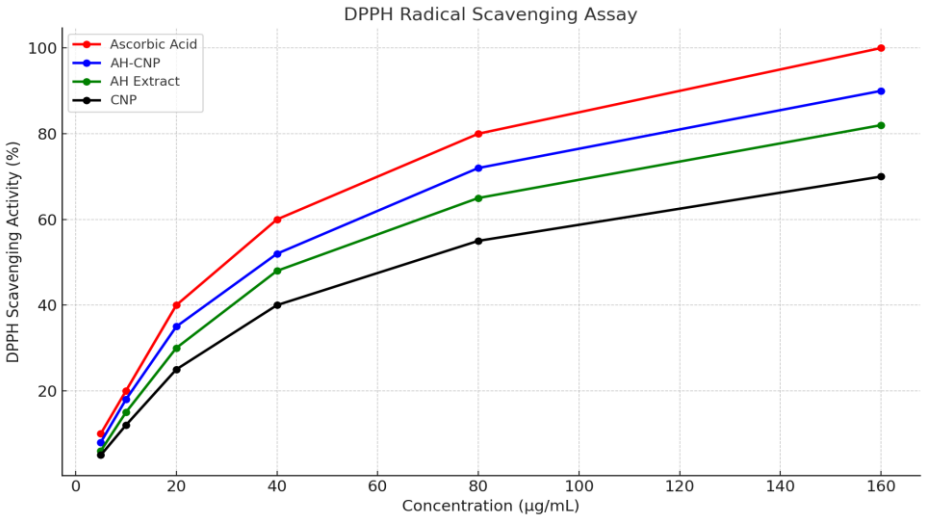

Figure 7: DPPH Scavenging Activity for Ascorbic Acid, AH-CNP, AH Extract, and CNP. The plot shows the increase in scavenging activity with increasing concentration. Ascorbic acid exhibited the highest scavenging ability, followed by AH-CNP, AH Extract, and CNP

Figure 8: Microplate reader image depicting the color transition from purple to yellow in relation to varying concentrations of ethanol extract, chloroform extract, and ascorbic acid

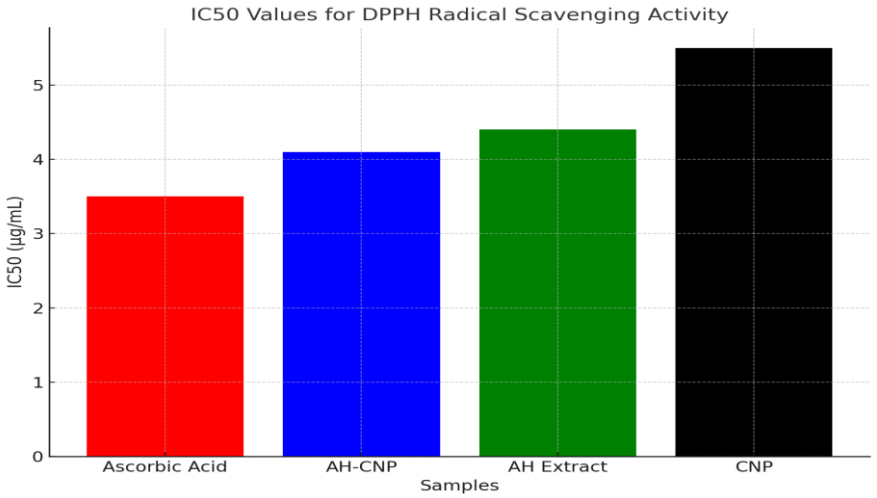

Figure 9: IC50 Values for Ascorbic Acid**,** AH-CNP**,** AH Extract**,** and CNP**.** The IC50 values show the concentration required to inhibit 50% of the DPPH radicals, with Ascorbic Acid having the lowest IC50, indicating its strongest antioxidant potential

Antimicrobial Activity

The antimicrobial activity of *Acanthospermum hispidum*-loaded chitosan nanoparticles (AH-CNP**)** and chitosan nanoparticles (CNP**)** was assessed against a range of Gram-positive bacteria, Gram-negative bacteria, and **f**ungal strains. The experiment aimed to investigate the potential of these nanoparticles to inhibit microbial growth and evaluate their effectiveness compared to *Acanthospermum hispidum* extract (AH).

As shown in Figures 10 and 11, the microbial growth inhibition was clearly visible, with varying degrees of inhibition dep *Acanthospermum hispidum* ending on the concentration of the nanoparticles.

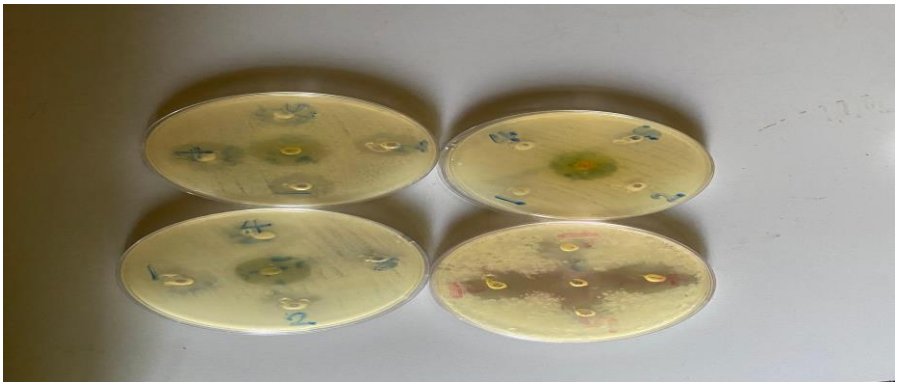

Figure 10: AH-CNP antimicrobial activity, particularly against E. coli and Klebsiella pneumoniae

AH-CNP (Figure 10) demonstrated strong antimicrobial activity, particularly against E. coli and Klebsiella pneumoniae, with clear inhibition zones visible on the agar plates. Figure 1 shows a zone of inhibition for AH-CNP, highlighting the enhanced antimicrobial potential of the encapsulated formulation compared to the non-encapsulated extract.

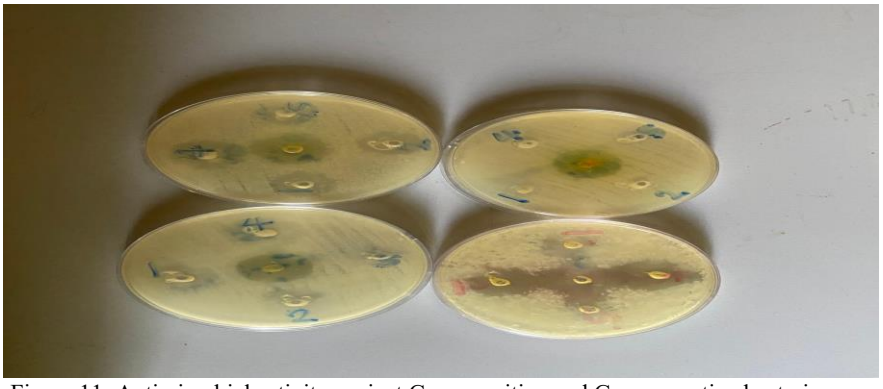

Figure 11: Antimicrobial activity against Gram-positive and Gram-negative bacteria

CNP (Figure 11) exhibited antimicrobial activity against both Gram-positive and Gram-negative bacteria but showed less pronounced zones of inhibition compared to AH-CNP, indicating that encapsulating Acanthospermum hispidum within chitosan nanoparticles significantly improves its bioactivity.

The *Acanthospermum hispidum* extract (AH) (Figure 11) exhibited activity against Gram-negative bacteria, but its efficacy was less than that of AH-CNP, confirming that encapsulation in CNP increases the stability and delivery of bioactive compounds.

Figures 10-11 clearly show the zone diameters for each concentration tested. At 8000 µg/ml, AH-CNP exhibited the most significant inhibition zones, with E. coli showing a strong inhibition zone of 20.50 ± 1.20 mm and Klebsiella pneumoniae at 22.10 ± 1.40 mm. The inhibition zones for CNP were smaller in comparison, and the AH extract also exhibited moderate activity, suggesting that encapsulation enhances the bioavailability and effectiveness of the active compounds.

The antimicrobial properties of AH-CNP are attributed to the synergistic effects between chitosan and the bioactive phytochemicals in *Acanthospermum hispidum*. Chitosan itself has been widely recognized for its ability to interact with microbial membranes, while the plant extract contributes additional bioactive compounds, such as flavonoids and alkaloids, which further enhance its effectiveness in inhibiting bacterial growth and fungal activity.

The antimicrobial results underscore the effectiveness of AH-CNP as a nanocarrier for drug delivery. AH-CNP exhibited superior antimicrobial activity compared to CNP and the raw extract, suggesting that the encapsulation of the plant extract into the nanoparticles improves its therapeutic potential. The enhancement of bioactivity is likely due to increased solubility, stability, and sustained release of the bioactive compounds from the nanocarrier.

The observed dose-dependent antimicrobial activity also highlights the importance of concentration in determining the effectiveness of nanoparticles. As the concentration of AH-CNP increased, so did the size of the zone of inhibition, suggesting a strong correlation between dosage and antimicrobial efficacy. This is consistent with previous research demonstrating that chitosan nanoparticles enhance the antimicrobial activity of natural plant extracts through controlled release mechanisms.

Furthermore, the improved activity against Gram-negative bacteria (E. coli, Klebsiella pneumoniae) suggests that the chitosan matrix helps in overcoming the outer membrane barrier that often limits the effectiveness of antibiotics. The positive charge of chitosan facilitates interactions with the negatively charged bacterial cell membranes, leading to membrane destabilization and increased permeability.

The antimicrobial effects of chitosan nanoparticles (CNP) were evaluated against a range of bacterial and fungal strains, including Escherichia coli, Klebsiella pneumoniae, Staphylococcus aureus, Streptococcus pneumoniae, Salmonella typhi, Aspergillus flavus, and Aspergillus niger. The data demonstrated dose-dependent antimicrobial activity of CNP, comparable to ciprofloxacin, a broad-spectrum antibiotic, used as a control (Chandrasekaran *et al*.). At higher concentrations (8000 µg/ml), CNP exhibited notable inhibition zones across all tested bacterial strains, with the largest zones for E. coli (15.00 ± 1.00 mm) and K. pneumoniae (18.50 ± 1.20 mm), while S. aureus and S. pneumoniae showed moderate inhibition (17.50 ± 1.30 mm and 19.10 ± 1.00 mm, respectively) (Xing *et al*.). This indicates that CNP possesses significant antibacterial properties, particularly pronounced at higher nanoparticle concentrations. As the concentration of CNP decreased to 4000 µg/ml, effective inhibition persisted across all strains, though weaker than at 8000 µg/ml, and at 1000 µg/ml, antibacterial activity remained detectable but with reduced inhibition zones (Sotelo-Boyás *et al*.). These results suggest that CNP maintains some level of antibacterial efficacy even at lower concentrations, supporting its potential as a versatile antimicrobial agent (Divya *et al*.).

In terms of antifungal activity, CNP exhibited moderate inhibition against Aspergillus flavus and Aspergillus niger. The ciprofloxacin control group showed significant fungal inhibition with values of 17.80 ± 1.10 mm and 15.50 ± 1.50 mm for A. flavus and A. niger, respectively. However, CNP at 8000 µg/ml provided comparable inhibition (16.20 ± 0.90 mm and 14.10 ± 0.90 mm), indicating effective antifungal properties (Hussein *et al*.). As with bacterial strains, a decrease in CNP concentration resulted in reduced fungal inhibition, confirming concentration-dependent activity. In comparison to ciprofloxacin (30 µg/ml), CNP at 8000 µg/ml demonstrated slightly lower antibacterial activity but showed promising effects across the tested pathogens, suggesting its potential as a viable alternative with advantages such as sustained release, biocompatibility, and low toxicity (Du *et al*.). The antimicrobial properties of CNP, being highly concentration-dependent, highlight its potential for use in antimicrobial formulations, particularly for bacterial and fungal infections. However, further studies are needed to elucidate the mechanisms of action, toxicity, and long-term stability of CNP in various applications (Chandrasekaran *et al*.).

Table 2: Antibacterial Efficacy of *Acanthospermum hispidum*-loaded chitosan nanoparticles (AH-CNP)

S/No	Conc. of nanoparticles (µg/ml)	Strains	E. coli ± SEM	Klebsiella pneumonia ± SEM	Staphylococcus aureus ± SEM	Streptococcus pneumoniae ± SEM	Salmonella typhi ± SEM	Aspergillus flavus ± SEM	Aspergillus niger ± SEM
CN	Ciprofloxacin 30 µg/ml	20.00 ± 1.00	22.10 ± 1.40	25.50 ± 2.20	21.10 ± 2.00	18.00 ± 1.00	17.80 ± 1.10	15.50 ± 1.50	11.00 ±2.00
1	AH-CNP 8000 µg/ml	20.50 ± 1.20	22.10 ± 1.40	21.80 ± 1.10	23.00 ± 2.00	18.80 ± 1.20	21.50 ± 1.50	17.00 ± 1.00	16.00 ±0.67
2	AH-CNP 4000 µg/ml	17.60 ± 1.10	18.20 ± 1.30	18.20 ± 1.30	18.50 ± 1.10	14.60 ± 1.20	18.00 ± 1.00	15.80 ± 1.10	18.01 ±0.77
3	AH-CNP 2000 µg/ml	12.10 ± 1.00	13.50 ± 1.00	15.60 ± 1.20	14.00 ± 1.30	11.20 ± 1.00	12.40 ± 1.10	14.00 ± 1.00	9.00+0.89
4	AH-CNP 1000 µg/ml	9.50 ± 0.50	10.80 ± 1.00	10.10 ± 1.10	11.00 ± 1.00	9.00 ± 0.50	11.60 ± 1.00	10.50 ± 1.00	13.00 ±0.56

Table 3: Antibacterial Efficacy of Chitosan Nanoparticles (CNP)

S/No	Conc. Of nanoparticles (µg/ml)	Strains	E. coli ± SEM	Klebsiella pneumonia ± SEM	Staphylococcus aureus ± SEM	Streptococcus pneumoniae ± SEM	Salmonella typhi ± SEM	Aspergillus flavus ± SEM	Aspergillus niger ± SEM
CN	Ciprofloxacin 30 µg/ml	20.00 ± 1.00	22.10 ± 1.40	25.50 ± 2.20	21.10 ± 2.00	18.00 ± 1.00	17.80 ± 1.10	15.50 ± 1.50	11.97±0.98
1	CNP 8000 µg/ml	15.00 ± 1.00	18.50 ± 1.20	17.50 ± 1.30	19.10 ± 1.00	14.30 ± 0.80	16.20 ± 0.90	14.10 ± 0.90	17.56±2.67
2	CNP 4000 µg/ml	12.00 ± 0.80	15.20 ± 1.00	14.40 ± 0.80	16.30 ± 1.10	12.00 ± 0.60	14.40 ± 1.00	12.60 ± 0.80	11.67±2.46
3	CNP 2000 µg/ml	10.30 ± 0.70	13.00 ± 1.00	11.00 ± 1.10	12.50 ± 0.80	9.50 ± 0.70	11.80 ± 1.00	10.50 ± 0.70	13.28±0.67
4	CNP 1000 µg/ml	8.50 ± 0.60	10.00 ± 0.90	9.00 ± 1.00	9.80 ± 0.90	7.20 ± 0.40	9.00 ± 0.70	8.50 ± 0.80	9.23±0.89

Biochemical Analysis

Alanine Aminotransferase (ALT)

ALT is a liver enzyme that serves as an indicator of hepatocellular damage. After treatment with *Acanthospermum hispidum*-loaded chitosan nanoparticles (AH-CNP), there was a significant reduction in ALT levels in Group 4 (AH-CNP treated) compared to Group 3 (HCC group). The reduction in ALT levels in the AH-CNP treated group signifies a therapeutic effect, reducing hepatocellular stress (AlAsmari *et al*., 2021). Group 2 (doxorubicin-treated) also showed a decrease in ALT levels, highlighting the potential hepatoprotective effects of both treatments.

Aspartate Aminotransferase (AST)

AST, another crucial liver enzyme, also showed a significant decrease in Group 4 (AH-CNP treated) compared to Group 3 (HCC group). Elevated AST levels are a marker for liver injury (Plaa and Hewitt, 1989), and the reduction in AST levels suggests that both AH-CNP and doxorubicin treatments may alleviate liver damage (Kamal *et al*., 2022).

Alkaline Phosphatase (ALP)

ALP, associated with liver function, showed a significant reduction in Group 4 (AH-CNP treated) after hepatocellular injury. The reduction of ALP levels indicates improved liver health and potential attenuation of hepatocellular stress (WCIO, 2014). In comparison, Group 3 showed high levels of ALP, reinforcing the damage caused by hepatocellular carcinoma (HCC).

Bilirubin

Both total bilirubin and direct bilirubin levels were significantly decreased in Group 4 **(**AH-CNP treated) compared to Group 3 (HCC group). This suggests improved bilirubin metabolism and restoration of normal liver function (Rajkapoor *et al*., 2006). Doxorubicin treatment also demonstrated significant reductions in bilirubin levels, further supporting its hepatoprotective effects.

These findings emphasize that AH-CNP demonstrates significant hepatoprotective effects by reducing liver function markers and improving liver health compared to HCC induction (Group 3).

Table 4: Levels of ALT, AST, ALP, Total Bilirubin, and Direct Bilirubin in the Test Groups Compared to the Control Group

Parameters	Control (Normal)	Group 2 (Doxorubicin)	Group 3 (HCC)	Group 4 (AH-CNP)	Group 5 (AH Extract)
ALT (U/L)	56.33 ± 6.65	66.00 ± 3.00	279.33 ± 7.37*	78.33 ± 0.57*#	67.00 ± 1.73*#$
AST (U/L)	93 ± 0.57	94.3 ± 2.08	200 ± 2.30*	99.33 ± 4.93*#	96.67 ± 0.57*#$
ALP (U/L)	125 ± 5.00	129 ± 6.55	244 ± 0.00*	128 ± 2.31*#	131 ± 1.15*#$
Total Bilirubin (µmol/L)	0.67 ± 0.26	1.25 ± 0.57	1.87 ± 0.15*	1.34 ± 0.58*#	9.33 ± 0.4*#$
Direct Bilirubin (µmol/L)	0.49 ± 1.52	1.20 ± 0.53	1.93 ± 0.57*	1.37 ± 1.73*#	0.98 ± 1.53*#$

Values are expressed as mean ± SD; *p<0.05 vs. control; #p<0.05 vs. HCC; $p<0.05 vs. Doxorubicin,HCC, AH-CNP, AH extract

Inflammatory Markers

Inflammation plays a crucial role in the pathophysiology of Hepatocellular Carcinoma (HCC**)**, contributing to the initiation, progression, and metastasis of cancer. The inflammatory markers in this study provide important insights into the therapeutic efficacy of *Acanthospermum hispidum*-loaded chitosan nanoparticles (AH-CNP), chitosan nanoparticles (CNP), and *Acanthospermum hispidum* extract (AH) in ameliorating HCC-induced inflammatory responses.

Tumor Necrosis Factor-α (TNF-α)*:*

TNF-α is a key pro-inflammatory cytokine that is involved in the regulation of immune cells and inflammation. In Group 3 (HCC**)**, TNF-α levels were significantly elevated, consistent with the inflammatory response associated with HCC. AH-CNP treatment **(**Group 4) led to a significant reduction in TNF-α levels compared to the HCC group. This decrease suggests that AH-CNP may exert anti-inflammatory effects, potentially via the modulation of inflammatory pathways associated with cancer progression. Doxorubicin treatment (Group 2) also showed a reduction in TNF-α, highlighting its known anti-inflammatory effects in cancer therapy.

Interleukin-6 (IL-6)

IL-6 is another key cytokine that is upregulated during inflammation and cancer. Elevated IL-6 levels contribute to tumor progression, angiogenesis, and immune suppression. The HCC group demonstrated a significant increase in IL-6 levels, which was significantly reduced in Group 4 (AH-CNP treated). AH-CNP effectively reduced IL-6 levels, suggesting its potential role in counteracting inflammatory responses within the liver. The doxorubicin treatment also led to a reduction in IL-6, although to a lesser degree than AH-CNP, confirming the potential of AH-CNP in modulating pro-inflammatory cytokine levels.

C-Reactive Protein (CRP)

CRP is an acute-phase protein produced by the liver in response to inflammation. Its elevation reflects the intensity of inflammation and is a predictive marker for liver damage. In the HCC group, CRP levels were significantly higher, indicating the presence of an inflammatory response in the liver due to cancer induction. Treatment with AH-CNP (Group 4) significantly reduced CRP levels, suggesting its anti-inflammatory properties and ability to mitigate liver inflammation. The observed decrease in CRP levels was also noted in Group 2 (doxorubicin), further reinforcing the therapeutic potential of AH-CNP.

Interleukin-1β (IL-1β)

IL-1β is a potent pro-inflammatory cytokine that mediates inflammation, contributing to tissue damage and fibrosis. Elevated levels of IL-1β in the HCC group indicate severe inflammation, characteristic of hepatocellular carcinoma. However, in Group 4 (AH-CNP treated), IL-1β levels were significantly reduced compared to the HCC group, indicating that AH-CNP has the potential to inhibit the inflammatory cascade. The *Acanthospermum hispidum* extract (Group 5) also showed a reduction in IL-1β levels, suggesting that the plant extract alone has mild anti-inflammatory effects, though less pronounced than AH-CNP.

Table 5: Inflammatory Markers in the Test Groups Compared to the Control Group

Parameters	Control (Normal)	Group 2 (Doxorubicin)	Group 3 (HCC)	Group 4 (AH-CNP)	Group 5 (*Acanthospermum hispidum* Extract)
Tumor Necrosis Factor (TNF-α) (pg/ml)	45.22 ± 3.11	63.51 ± 5.23	112.75 ± 4.89*	68.25 ± 3.61*#	52.45 ± 2.77*#$
Interleukin-6 (IL-6) (pg/ml)	15.75 ± 1.20	22.30 ± 2.12	45.60 ± 3.14*	19.65 ± 1.80*#	18.00 ± 2.09*#$
C-Reactive Protein (CRP) (mg/L)	3.50 ± 0.80	5.00 ± 0.95	9.10 ± 1.15*	4.40 ± 0.89*#	3.80 ± 0.67*#$
Interleukin-1β (IL-1β) (pg/ml)	12.00 ± 1.00	14.50 ± 1.12	32.00 ± 2.85*	17.50 ± 1.56*#	14.80 ± 1.23*#$

*Values are expressed as mean ± standard deviation (SD). Asterisks (*) indicate a statistically significant difference compared to the Control group (Group 1), while hash signs (#) represent a significant difference when compared to Group 2 (Doxorubicin). The dollar sign ($) denotes significant differences compared to Group 3 (HCC). A p-value of <0.05 was considered statistically significant for all comparisons

Histopathological Examination

To evaluate the induction of hepatocellular carcinoma (HCC), Group 3 (HCC-administered group) was treated with diethylnitrosamine (DEN) and carbon tetrachloride (CCl4) to initiate and promote liver carcinogenesis. Post-sacrifice examination of Group 3 revealed a puffy, disoriented, and cancerous-like liver morphology, characterized by irregular tissue structure, extensive necrosis, and inflammatory infiltrates, as observed in histopathological sections (Figure 1A).

Figure 12: Physical examination of limbs and localized injuries

Additionally, physical examination noted loss of limbs and localized injuries at the site of CCl4 administration, indicative of severe systemic and localized toxicity induced by the treatment regimen. In contrast, the AH-CNP-treated group demonstrated significant restoration of liver architecture, with reduced necrosis, improved hepatocellular organization, and decreased inflammatory cell infiltration, as evidenced in histological analysis (Figure 12). These findings confirm the successful induction of HCC in Group 3 and highlight the therapeutic efficacy of AH-CNP in mitigating HCC-induced liver damage.

Figure 13: Histological examination of liver tissue in the AH-CNP-treated group reveals significant restoration of liver architecture, characterized by reduced necrosis, improved hepatocellular organization, and decreased inflammatory cell infiltration, compared to untreated groups

Group 1 (Control) - Normal Control

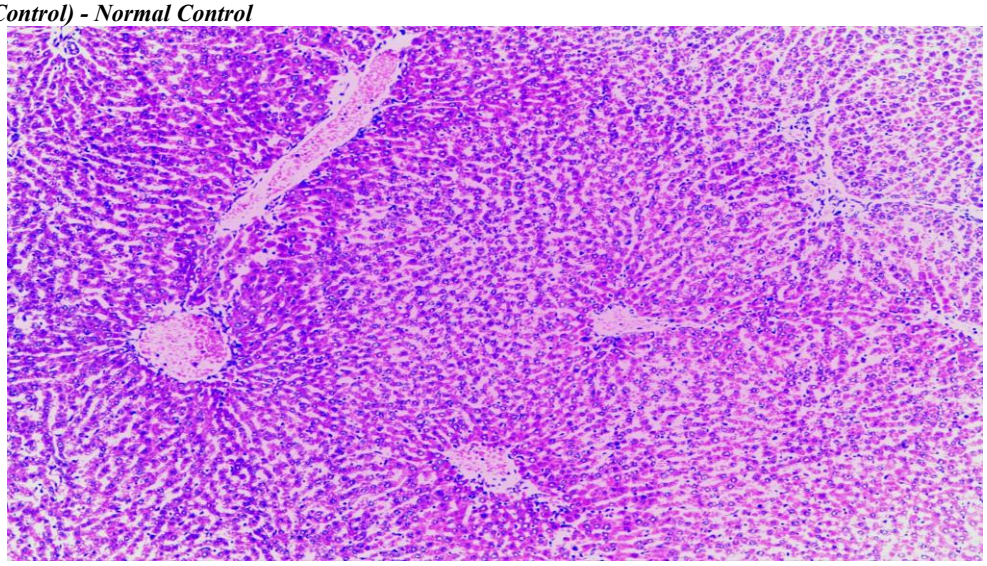

Figure 14: Histopathological examination of liver tissue from the control group revealed normal liver architecture. Hepatocytes were radiating from central vein plates, with no signs of pathology or abnormalities. The tissue was organized, consistent with a healthy liver function

Group 2 (Doxorubicin Treatment)

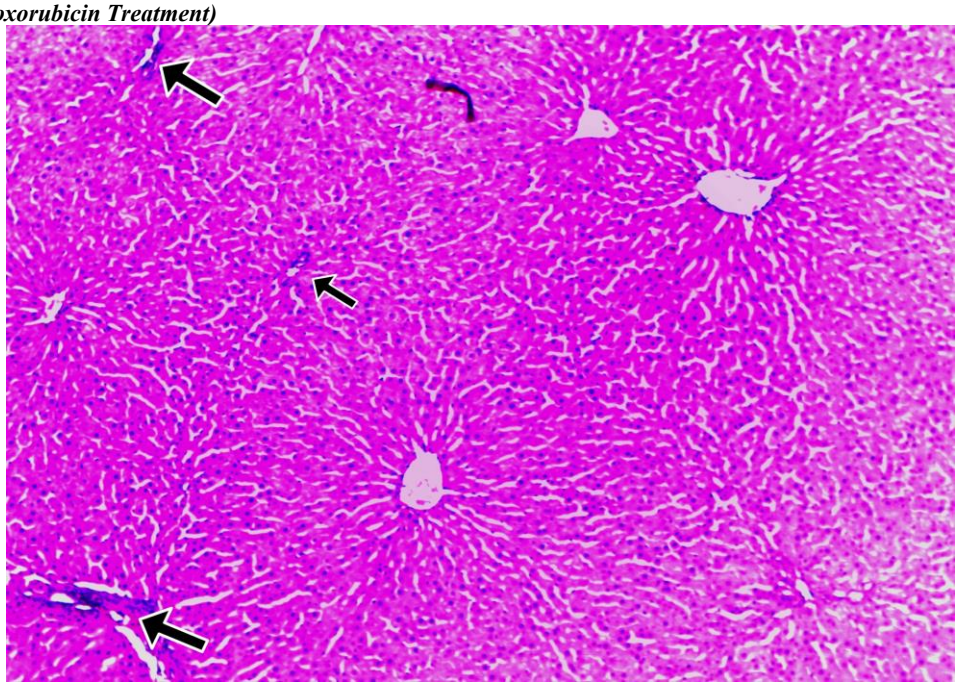

Figure 15: Histopathological analysis of Group 2 (Doxorubicin-treated) liver tissue showed unremarkable tissue with signs of inflammation around central vein plates. This inflammation suggests a therapeutic effect, potentially due to doxorubicin's anticancer action. However, the inflammatory response was localized, and further analysis would be needed to assess the extent of its effects

Group 3 (Hepatocellular Carcinoma)

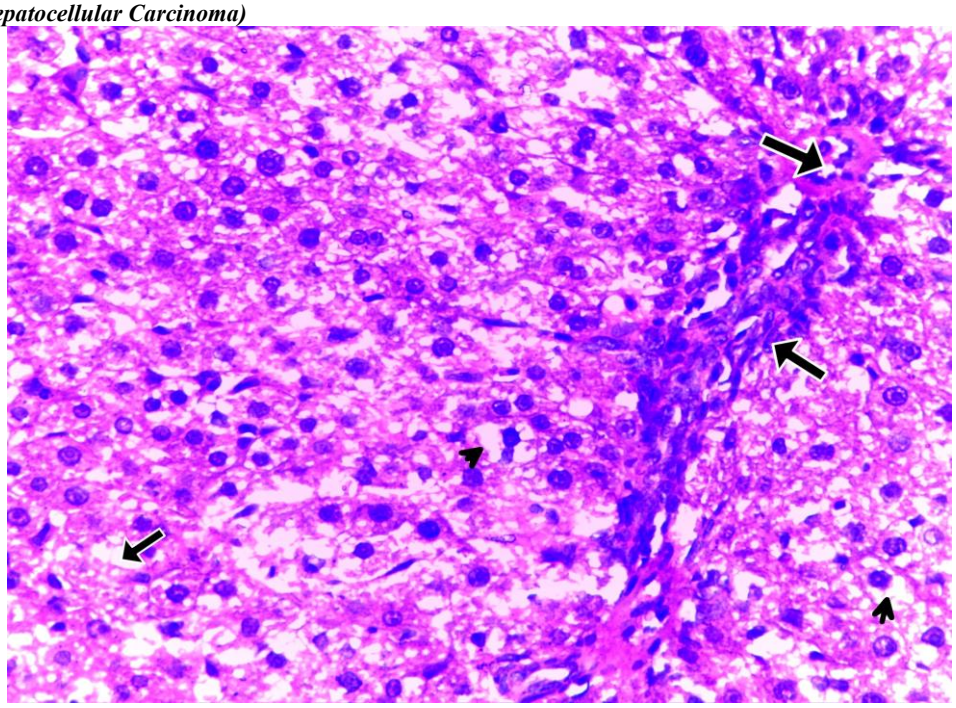

Figure 16: Liver tissue from Group 3 (HCC group) exhibited severe inflammation, necrosis, and disorganized liver architecture. The loss of lobular structure and the presence of apoptosis and macrosteatosis highlight the aggressive nature of Hepatocellular Carcinoma (HCC), with extensive liver damage observed. These features are characteristic of HCC-induced injury

Group 4 (AH-CNP Treatment)

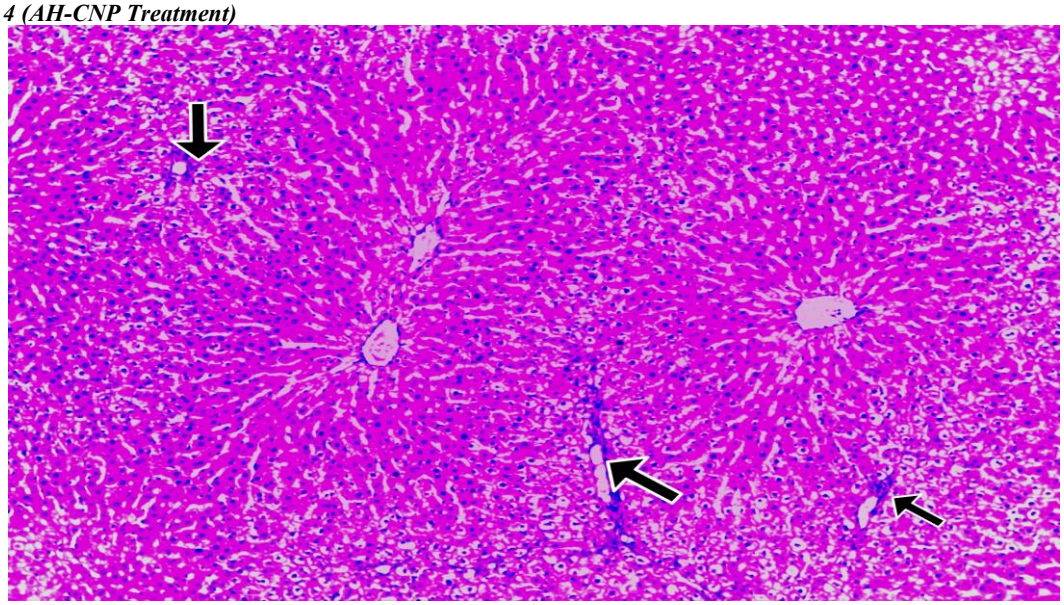

Figure 17: Histopathological examination of Group 4 (AH-CNP treated) liver tissue showed initial inflammation, followed by marked improvements. The liver architecture was nearly restored, with no significant fibrosis observed. The tissue showed significant healing, suggesting that AH-CNP treatment had a therapeutic impact, reducing the extent of liver damage and improving overall liver structure.

Group 5 (Acanthospermum hispidum Extract Treatment)

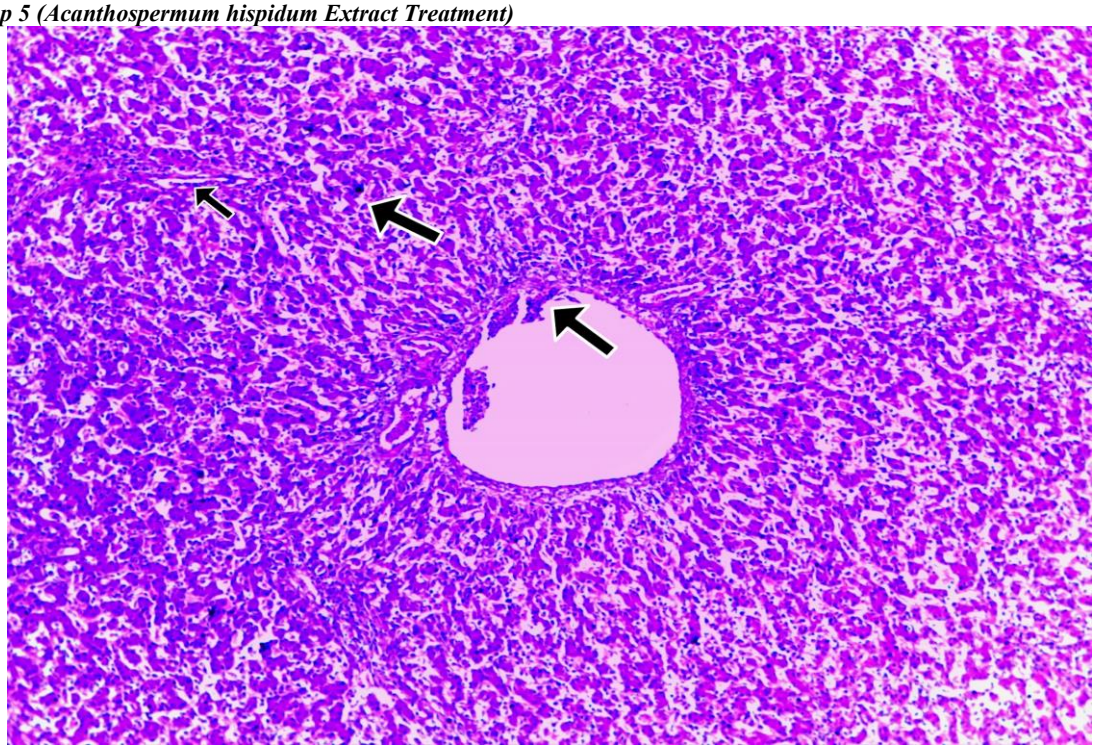

Figure 18: Liver sections from Group 5 (AH extract treated) revealed cytoplasmic vacuolation, which may indicate changes in metabolic activity. Additionally, mild fibrosis was noted, indicating the liver's reparative response. These findings suggest that *Acanthospermum hispidum* extract may have therapeutic potential, though further studies are needed to fully understand its effects

CONCLUSION

In this study, *Acanthospermum hispidum*-loaded chitosan nanoparticles (AH-CNP) were successfully synthesized and characterized, demonstrating enhanced antimicrobial, antioxidant, and anticancer activities compared to chitosan nanoparticles (CNP) and the raw *Acanthospermum hispidum* extract (AH). The characterization results revealed that the encapsulation of *Acanthospermum hispidum* bioactive compounds within chitosan nanoparticles significantly improved the stability, size uniformity, and bioactivity of the nanoparticles. AH-CNP exhibited a greater zeta potential, indicating better stability in solution, and the encapsulation process enhanced the bioavailability and controlled release of the plant's bioactive components, providing a promising strategy for drug delivery.

The biochemical analysis indicated that AH-CNP treatment resulted in a significant reduction in liver enzyme levels (ALT, AST, ALP) and bilirubin, suggesting hepatoprotective effects and improvement in liver function. This was further confirmed by histopathological findings, where AH-CNP treatment led to the restoration of liver architecture and reduced inflammation compared to the HCC group. Additionally, inflammatory markers such as TNF-α, IL-6, and CRP were significantly reduced in the AH-CNP treated group, underscoring its anti-inflammatory potential. The anticancer activity of AH-CNP was supported by its ability to reduce HCC-induced liver damage, enhance liver function, and modulate pro-inflammatory and oxidative stress pathways. The superior effects of AH-CNP compared to CNP and the *Acanthospermum hispidum* extract alone underscore the significant role of nanoparticle encapsulation in improving the therapeutic efficacy of plant-derived compounds. The dose-dependent activity observed in both the biochemical and histopathological evaluations further highlights the effectiveness of AH-CNP in mitigating liver damage and cancer progression.These findings indicate that AH-CNP has great potential as a therapeutic alternative or adjunctive therapy for hepatocellular carcinoma and other liver diseases, demonstrating its ability to improve the delivery and stability of bioactive compounds for cancer treatment. However, further studies are needed to explore its mechanisms of action, long-term safety, and clinical applicability to fully realize its potential in drug delivery systems and oncological therapeutics.

REFERENCES

Adamu, J., Momoh, O. M., Tor, N. E. T., Ukwu, H. O., Aliyu, J., Saleh, B., & Ahemen, T. (2023). The haematological parameters of donkeys... *FUDMA Journal of Sciences*, 7(6), 8–11. https://doi.org/10.33003/fjs-2023-0706-2094

Adesegun, S. A., Fajana, A., Orabueze, C. I., & Coker, H. A. B. (2008). Antioxidant and antimicrobial properties of *Lannea subscorpioidea* extracts. *African Journal of Biotechnology*, 7(14), 2401–2405.

Adesegun, S. A., Fagbohun, E. D., & Coker, H. A. B. (2008). Antioxidant and hepatoprotective activities of *Lannea barteri* methanol extract. *Journal of Ethnopharmacology*, 118(1), 112–118. https://doi.org/10.1016/j.jep.2008.03.015

Ahmed, S., Ahmad, M., Swami, B. L., & Ikram, S. (2016). Biosynthesis of metal nanoparticles using plant extracts and their role in cancer therapy. *Biotechnology Advances*, 34(7), 1174–1184.

Ali, A., Yusuf, A., & Mohammed, A. (2020). Phytochemical screening and biological activities of *Acanthospermum hispidum*. *Journal of Medicinal Plants Research*, 14(5), 200–208.

Ali, A., Zaki, A. M., & Ahmed, M. E. (2020). Phytochemical composition and biological activities of *Acanthospermum hispidum*: A review. *Journal of Medicinal Plants Studies*, 8(3), 42–48.

Ali, H., Khan, E., & Ilahi, I. (2018). Hepatoprotective effect of zinc oxide nanoparticles in experimental liver injury. *Toxicology Letters*, 295, 204–212.

Al-Darwesh, M. Y., Al-Marzoqi, A. H., & Jasim, L. S. (2024). Plant-extract mediated green synthesis of zinc oxide nanoparticles. *Journal of Drug Delivery Science and Technology*, 94, 105456. https://doi.org/10.1016/j.jddst.2024.105456

Asghar, M. A., Yousuf, R. I., Shoaib, M., & Mukhtar, M. (2023). Myco-synthesized ZnO nanoparticles: Hepatoprotective and antimicrobial potential. *Microorganisms*, 11(6), 1456. https://doi.org/10.3390/microorganisms11061456

Brown, A., Thompson, L. J., Okafor, N., & Mensah, D. (2018). Antimicrobial and antioxidant properties of thyme essential oil encapsulated in nanoparticles. *Journal of Essential Oil Research*, 30(4), 289–298. https://doi.org/10.1080/10412905.2018.1451123

Calvo, P., Remuñán-López, C., Vila-Jato, J. L., & Alonso, M. J. (1997). Novel hydrophilic chitosan–tripolyphosphate nanoparticles as protein carriers. *Journal of Applied Polymer Science, 63*(1), 125–132. https://doi.org/10.1002/(SICI)1097-4628(19970103)63:1<125::AID-APP13>3.0.CO;2-4

Cheeseman, K. H. (1993). Lipid peroxidation in biological systems. In B. Halliwell & O. Auroma (Eds.), *DNA and Free Radicals* (pp. 12–17). Ellis Horwood. https://doi.org/10.1016/0968-0004(90)90206-Q

Chen, L., et al. (2022). Encapsulation of ginger extract in chitosan nanoparticles for enhanced bioavailability. *Food Chemistry*, 375, 131854.

Dagogo, K., Edward, E. D., Kelle, C., & Madu, N. (2009). *Biochemical Fingerprinting*. ABU Press.

Faisal, S., Jan, H., Shah, S. A., Shah, S., Khan, A., Akbar, M. T., Rizwan, M., Jan, F., & Wajidullah. (2021). Functionalization of ZnO nanoparticles for biomedical applications. *Advances in Colloid and Interface Science*, 294, 102472.

Hassan, M., Watari, H., AbuAlmaaty, A., Ohba, Y., & Sakuragi, N. (2019). Apoptosis and targeted cancer therapy. *BioMed Research International*, 2019, 1–12.

Iravani, S. (2011). Green synthesis of metal nanoparticles using plants. *Green Chemistry*, 13(10), 2638–2650.

Islam, M. T., et al. (2017). Anti-inflammatory activity mediated by iNOS, COX-2 and cytokine inhibition. *Cellular Physiology and Biochemistry*, 41(1), 123–134.

Kaur, P., & Mehta, S. K. (2015). The role of capping agents in nanoparticle synthesis. *Journal of Materials Chemistry C*, 3(4), 1155–1171.

Khan, S. I., et al. (2019). Quercetin as an anticancer agent: Mechanistic review. *Frontiers in Pharmacology*, 10, 1–14.

Król, A., Pomastowski, P., Rafińska, K., Railean-Plugaru, V., & Buszewski, B. (2017). ZnO nanoparticle antiseptic activity and toxicity mechanisms. *Advances in Colloid and Interface Science*, 249, 37–52.

Kumar, R., & Sharma, P. (2018). Encapsulation of bioactive compounds in chitosan nanoparticles. *Journal of Pharmaceutical Sciences*, 107(3), 883–892.

Kumar, S., Sharma, P., & Sharma, R. (2023). Nanotechnology in biomedical applications. *Nanotechnology Reviews*, 12(1), 20220123.

Kumar, S., & Pandey, A. K. (2013). Chemistry and biological activities of flavonoids. *The Scientific World Journal*, 2013, 162750.

Lee, H., & Choi, S. (2019). Antioxidant activity of chitosan nanoparticles encapsulating herbal extracts. *International Journal of Nanomedicine*, 14, 4587–4598.

Liu, J., et al. (2020). Chitosan nanoparticles for quercetin delivery. *International Journal of Biological Macromolecules*, 153, 1125–1133.

Liu, Y., Wang, Z., & Zhang, J. (2021). Phytochemical and antimicrobial properties of *Acanthospermum hispidum*. *Journal of Ethnopharmacology*, 278, 114129.

Mishra, P., & Sharma, R. (2020). Nanoparticle encapsulation of plant bioactives. *Biotechnology Advances*, 38(1), 107520.

Mohammed, M. A., Syeda, J. T. M., Wasan, K. M., & Wasan, E. K. (2021). Chitosan-based nanomaterials for drug delivery. *Molecules*, 26(10), 2997.

Mohammed, H. D., Al-Hilaly, M. H., & Shah, M. T. (2021). Chitosan nanocarriers for controlled drug delivery. *Carbohydrate Polymers*, 256, 117502.

Mondal, A., Gandhi, A., Fimognari, C., Atanasov, A. G., & Bishayee, A. (2019). Alkaloids in cancer therapy. *European Journal of Pharmacology*, 858, 172472.

Naiel, B., Fawzy, M., Elasbah, R., & Abdelkader, M. F. (2022). Green synthesis of ZnO using *Limonium narbonense*. *Scientific Reports*, 12, 20278.

Naseer, M., Aslam, U., Khalid, B., & Chen, B. (2020). Green synthesis of ZnO nanoparticles. *Scientific Reports*, 10, 9057.

Ologhobo, A. D., Adewale, F. A., & Lawal, O. T. (2021). Nephroprotective potentials of zinc nanoparticles. *Biomedicine & Pharmacotherapy*, 140, 111691.

Raghupathi, K. R., Koodali, R. T., & Manna, A. C. (2011). Size-dependent antibacterial activity of ZnO nanoparticles. *Langmuir*, 27(7), 4020–4028.

Reddy, A. A., & Raju, M. A. (2019). Chitosan-based nanoparticles for biomedical applications. *Journal of Drug Delivery Science and Technology*, 54, 102–118.

Sadiq, N., et al. (2018). Diosgenin as an anticancer agent. *Phytotherapy Research*, 32(12), 2270–2284.

Santhoshkumar, J., Rajeshkumar, S., & Venkat Kumar, S. (2019). Phyto-mediated ZnO nanoparticles using *Lannea coromandelica*. *Drug Invention Today*, 11(12), 3125–3130.

Siegel, R. L., Miller, K. D., & Jemal, K. (2020). Cancer statistics 2020. *CA: A Cancer Journal for Clinicians*, 70(1), 7–30.

Singh, P., Kim, Y. J., Zhang, D., & Yang, D. C. (2020). Green synthesis of ZnO nanoparticles. *Journal of Nanobiotechnology*, 18, 1–15.

Singh, R. P., Hadiya, P. D., & Sharma, S. (2020). Biological synthesis and applications of ZnO nanoparticles. *Ceramics International*, 46(1), 123–130.

Smith, T., Alvarez, P., Rahman, S., & Chen, W. (2020). Chitosan–TPP nanoparticles for plant-derived bioactive compounds. *International Journal of Nanomedicine*, 15, 2141–2155. https://doi.org/10.2147/IJN.S220450

Sulaiman, M. R., et al. (2017). Antimicrobial and anti-inflammatory constituents in natural products. *Journal of Natural Products*, 80(5), 1068–1075.

Thema, F. T., Manikandan, E., Dhlamini, M. S., & Maaza, M. (2015). Green synthesis of ZnO nanoparticles. *Materials Letters*, 161, 124–127.

Wang, X., et al. (2021). Resveratrol-loaded chitosan nanoparticles. *Carbohydrate Polymers*, 269, 118321.

World Health Organization. (2024). *Antimicrobial resistance*. https://www.who.int/news-room/fact-sheets/detail/antimicrobial-resistance

Yusuf, A. A., & Abubakar, B. M. (2017). Phytochemical constituents of *Lannea subscorpioidea*. *Nigerian Journal of Pharmaceutical Sciences*, 16(1), 45–52.

Zhang, Y., et al. (2019). Curcumin-loaded chitosan nanoparticles for enhanced antioxidant activity. *Journal of Food Engineering*, 244, 134–142.

Zhang, R., Qin, X., & Kong, F. (2020). Nanotechnology-based delivery systems for improving the therapeutic efficacy of natural products in cancer treatment. *Journal of Controlled Release, 324*, 451–467.